Atmos. Chem. Phys., 14, 765–781, 2014
www.atmos-chem-phys.net/14/765/2014/
doi:10.5194/acp-14-765-2014
© Author(s) 2014. CC Attribution 3.0 License.

Atmospheric Chemistry and Physics
Open Access

Four years of ground-based MAX-DOAS observations of HONO and NO_2 in the Beijing area

F. Hendrick[1], J.-F. Müller[1], K. Clémer[1,*], P. Wang[2], M. De Mazière[1], C. Fayt[1], C. Gielen[1], C. Hermans[1], J. Z. Ma[3], G. Pinardi[1], T. Stavrakou[1], T. Vlemmix[1,4], and M. Van Roozendael[1]

[1]Belgian Institute for Space Aeronomy (BIRA-IASB), Brussels, Belgium
[2]Institute of Atmospheric Physics, Chinese Academy of Science, Beijing, China
[3]Chinese Academy of Meteorological Sciences, Beijing, China
[4]Delft University of Technology (TU-Delft), Delft, the Netherlands
[*]now at: Instituut voor Sterrenkunde, Katholieke Universiteit Leuven, Leuven, Belgium

Correspondence to: F. Hendrick (franch@oma.be)

Received: 26 March 2013 – Published in Atmos. Chem. Phys. Discuss.: 22 April 2013
Revised: 12 December 2013 – Accepted: 13 December 2013 – Published: 22 January 2014

Abstract. Ground-based Multi-Axis Differential Optical Absorption Spectroscopy (MAX-DOAS) measurements of nitrous acid (HONO) and its precursor NO_2 (nitrogen dioxide) as well as aerosols have been performed daily in Beijing city centre (39.98° N, 116.38° E) from July 2008 to April 2009 and at the suburban site of Xianghe (39.75° N, 116.96° E) located ∼ 60 km east of Beijing from March 2010 to December 2012. This extensive dataset allowed for the first time the investigation of the seasonal cycle of HONO as well as its diurnal variation in and in the vicinity of a megacity. Our study was focused on the HONO and NO_2 near-surface concentrations (0–200 m layer) and total vertical column densities (VCDs) and also aerosol optical depths (AODs) and extinction coefficients retrieved by applying the Optimal Estimation Method to the MAX-DOAS observations. Monthly averaged HONO near-surface concentrations at local noon display a strong seasonal cycle with a maximum in late fall/winter (∼ 0.8 and 0.7 ppb at Beijing and Xianghe, respectively) and a minimum in summer (∼ 0.1 ppb at Beijing and 0.03 ppb at Xianghe). The seasonal cycles of HONO and NO_2 appear to be highly correlated, with correlation coefficients in the 0.7–0.9 and 0.5–0.8 ranges at Beijing and Xianghe, respectively. The stronger correlation of HONO with NO_2 and also with aerosols observed in Beijing suggests possibly larger role of NO_2 conversion into HONO in the Beijing city center than at Xianghe. The observed diurnal cycle of HONO near-surface concentration shows a maximum in the early morning (about 1 ppb at both sites) likely resulting from night-time accumulation, followed by a decrease to values of about 0.1–0.4 ppb around local noon. The HONO / NO_2 ratio shows a similar pattern with a maximum in the early morning (values up to 0.08) and a decrease to ∼ 0.01–0.02 around local noon. The seasonal and diurnal cycles of the HONO near-surface concentration are found to be similar in shape and in relative amplitude to the corresponding cycles of the HONO total VCD and are therefore likely driven mainly by the balance between HONO sources and the photolytic sink, whereas dilution effects appear to play only a minor role. The estimation of OH radical production from HONO and O_3 photolysis based on retrieved HONO near-surface concentrations and calculated photolysis rates indicate that in the 0–200 m altitude range, HONO is by far the largest source of OH radicals in winter as well as in the early morning at all seasons, while the contribution of O_3 dominates in summer from mid-morning until mid-afternoon.

1 Introduction

Since the late 1970s, nitrous acid (HONO) has been identified as a key chemical species in the troposphere, especially through its photolysis which leads to the formation of the hydroxyl radical OH (Perner and Platt, 1979). OH is known as the major oxidant (“detergent”) of the atmosphere responsible for the degradation of most pollutants. It contributes also to the formation of ozone and PANs (peroxyacyl nitrates)

causing the so-called "photochemical smog" in polluted regions, as well as to the formation of aerosol particles from the oxidation of volatile organic compounds (VOCs). The photochemistry of HONO has been and is still extensively discussed in the literature (see e.g., Sörgel et al., 2011a; Li et al., 2012; Elshorbany et al., 2012). The heterogeneous conversion of nitrogen dioxide (NO_2) on wet organic and inorganic ground surfaces (soil, buildings, vegetation, and aerosols) is believed to be a major source of HONO, and very probably its main source during the night (Wojtal et al., 2011 and references therein):

$$2NO_2 + H_2O + \text{surface} \rightarrow HONO + HNO_3 \quad \text{(R1)}$$

Recent field studies and laboratory measurements have identified other heterogeneous daytime sources like photosensitized reduction of NO_2 on organic surfaces (George et al., 2005; Stemmler et al., 2006) and the photolysis of adsorbed nitric acid/nitrate at UV wavelengths (Zhou et al., 2003). Su et al. (2011) also showed that soil, through nitrite-producing microbes, can release important HONO amounts. Other HONO sources are direct emissions from combustion processes and the following gas-phase reaction:

$$NO + OH + M \rightarrow HONO + M \quad \text{(R2)}$$

Reaction (R2) operates only during daytime, when the OH and NO concentrations are high. HONO sinks include dry deposition during nighttime, and photolysis (Reaction R3) during daytime, at a rate close to $10^{-3}\,s^{-1}$ around noon (see Sect. 3.3):

$$HONO + h\nu(\lambda < 400\,\text{nm}) \rightarrow OH + NO \quad \text{(R3)}$$

$$HONO + OH \rightarrow H_2O + NO_2 \quad \text{(R4)}$$

The reaction of HONO with OH (Reaction R4) is comparatively very slow. The rapid photolysis of HONO accumulated during the night is the main source of OH radicals in early morning when other radical sources, i.e. the photolysis of ozone and carbonyls, are still weak. It should be noted that recent measurements in the Los Angeles Basin have suggested that nitryl chloride ($ClNO_2$) can be, together with HONO, an important source of radicals in the morning in urban environments (Young et al., 2012). This study also showed that vertical gradients of radical precursors should be taken into account in radical budgets, especially in case of HONO.

Despite the numerous field campaigns and laboratory experiments conducted during the last three decades, the main HONO formation mechanisms are still not fully characterised, and their relative contributions to the observed HONO concentrations are not well quantified. Model simulations accounting only for anthropogenic emissions and the known gas phase formation through Reaction (R2) generally largely underestimate the measured daytime HONO levels, with possibly important consequences for the prediction of oxidants (OH, O_3, PANs) (e.g., Kleffmann et al., 2005; Sörgel et al., 2011b). Consequently, the largely unknown HONO daytime source can have a significant impact on air quality and chemistry-climate modeling (Elshorbany et al., 2012 and references therein).

So far, HONO has been measured mainly using the long-path DOAS (Differential Optical Absorption Spectroscopy) and in-situ LOPAP-like (Long-Path Absorption Photometer) techniques. LOPAP is a wet chemical technique based on the dissolution of HONO in the liquid phase as nitrite (NO_2^-) followed by its detection as an azo dye (compound bearing the $R-N=N-R'$ functional group) with a long-path absorption photometer (Heland et al., 2001; Kleffmann et al., 2002). The LOPAP instruments can generally be operated only for a limited period of time, from a few weeks to a couple of months, due to instrumental and logistics issues. Long-path DOAS is an active (i.e. using an artificial light source) DOAS technique consisting of the measurement of the trace gas concentration integrated along a light path of several hundred metres to a few kilometres between the light source and the spectrometer (Hönninger et al., 2004; Platt and Stutz, 2008). The first detection of HONO by long-path DOAS was made over the Los Angeles air basin in the late 1970s (Perner and Platt, 1979). Both long-path DOAS and LOPAP show a high sensitivity to HONO and have the advantage to be independent of daylight, enabling nighttime measurements.

Here we present four years of ground-based Multi-Axis (MAX-) DOAS observations of HONO and its main precursor NO_2 and aerosols in the Beijing area from July 2008 till December 2012. It is the first time that measurements of HONO in or in the vicinity of a megacity are reported over such a long time period, allowing investigation of the seasonal variation of this species in urban conditions. MAX-DOAS is a passive DOAS technique based on measurements of scattered sunlight at zenith and at different elevation angles towards the horizon (the so-called off-axis geometry), increasing therefore the sensitivity to absorbers present close to the ground compared to the zenith scattered sunlight technique (Hönninger et al., 2004; Platt and Stutz, 2008). Due to the use of daylight and the need to minimise the contribution of the stratosphere for absorbers with strong stratospheric concentration like NO_2 here, our MAX-DOAS observations are performed from $\sim 85°$ SZA (solar zenith angle) sunrise to 85° SZA sunset with a time resolution of ~ 15 min (time needed for a complete MAX-DOAS scan). The instrumental set up including data transfer is fully automated, allowing continuous daily operation throughout the year. Moreover, by applying appropriate inversion methods like the Optimal Estimation (OEM; Rodgers, 2000), some information on the vertical distribution of the target trace gases can be retrieved in addition to the vertical column density (e.g., Hendrick et al., 2004; Hönninger et al., 2004; Wittrock et al., 2004; Friess et al., 2006; Clémer et al., 2010; Vlemmix et al., 2011). It should be noted that altitude-resolved measurements of trace gases are also possible with long-path DOAS

or in-situ techniques, generally with a better vertical resolution and signal-to-noise ratio than MAX-DOAS, but these require more sophisticated instrumental set up like, for example, placing retro-reflectors or in-situ instruments on different floors of a building (e.g. Stutz et al., 2002; Wang et al., 2006; Wong et al., 2012; Villena et al., 2011).

In the present study, MAX-DOAS observations of HONO, NO_2, and aerosols have been performed from July 2008 to April 2009 in the Beijing city centre (39.98° N, 116.38° E) and from March 2010 until December 2012 at the suburban site of Xianghe (39.75° N, 116.96° E) located ∼ 60 km east of Beijing. From these datasets, the diurnal and seasonal variations of the HONO and NO_2 vertical column densities (VCDs) and near-surface concentrations and aerosol optical depths (AODs) in the Beijing area are investigated. The OH production from HONO is also estimated based on the retrieved HONO concentrations and calculated photolysis rates. In Sect. 2, the MAX-DOAS measurements of HONO, NO_2, and aerosols are introduced, including a description of the instrumental set up, DOAS analysis settings, and vertical profile retrievals. HONO, NO_2, and AOD retrievals have been also verified through comparisons with correlative data. Section 3 presents the results: the seasonal variation of daytime HONO and NO_2 VCDs and near-surface concentrations and AODs, their diurnal variation and an estimation of the OH production from HONO and ozone. Concluding remarks are given in the last section.

2 MAX-DOAS measurements

2.1 Instrumental set up

The MAX-DOAS instrument used in this study has been extensively described in Clémer et al. (2010). It is a dual-channel system composed of two grating spectrometers covering the UV and visible wavelength ranges (300–390 nm and 400–720 nm, respectively). The output of both spectrometers is connected to cooled CCD detectors. The spectrometers and detectors are mounted inside a thermo-regulated box in order to minimise thermal stress on optical and mechanical parts. The instrument function is close to a Gaussian with a full width at half maximum (FWHM) of 0.4 nm and 0.9 nm for the UV and visible channels, respectively. Scattered light is collected at various elevation and azimuth angles by an optical head mounted on a commercial sun tracker (INTRA, Brusag) and the light is guided to the two spectrometers through optical fibres.

The instrument, which was designed and assembled at BIRA-IASB in Brussels, was installed during the July 2008–April 2009 period on the roof of the Institute of Atmospheric Physics (IAP) of the Chinese Academy of Sciences located in the Beijing city centre (39.98° N, 116.38° E). Then, it was moved to the suburban site of Xianghe (39.75° N, 116.96° E) located about 60 km east of Beijing where it has been operating continuously from March 2010 until now. At both locations, the azimuthal scan option was not activated and the telescope points towards a fixed azimuth direction (north). A full MAX-DOAS scan requires ∼ 15 min and comprises the following 9 elevation angles: 2°, 4°, 6°, 8°, 10°, 12°, 15°, 30°, and 90° (zenith).

2.2 DOAS analysis

The measured scattered light spectra are analysed using the spectral fitting software suite QDOAS developed at BIRA-IASB (http://uv-vis.aeronomie.be/software/QDOAS/). The principle of the DOAS technique is to separate the absorption of molecular species which usually display narrow features from a broadband background resulting mainly from Mie and Rayleigh scattering and instrumental effects (Platt and Stutz, 2008). The direct product of the DOAS spectral fitting method is the differential slant column density (DSCD) which is the concentration of a given absorber integrated along the effective light path relative to the amount of the same absorber in a measured reference spectrum. For profile retrieval in the troposphere, it is a common way to select the zenith measurement of a MAX-DOAS scan as the reference for the off-axis DSCDs of the same scan in order to minimise the stratospheric signal (Clémer et al., 2010; Peters et al., 2012). This is particularly important for NO_2 which displays a significant concentration in the stratosphere.

HONO DSCDs are retrieved in the 337–375 nm wavelength range, taking into account the spectral signature of NO_2 at 220 and 296 K (Vandaele et al., 1998), O_3 at 218 and 243 K (Brion et al., 2004), O_4 (Hermans et al., 2003), BrO at 223 K (Fleischmann et al., 2004), HCHO at 293 K (Meller and Moortgat, 2000), and the filling-in of the solar Fraunhofer bands by the Ring effect (Grainger and Ring, 1962). The HONO absorption cross-sections at 296 K are obtained from Stutz et al. (2000). A fifth-order polynomial is used to fit the low frequency spectral structure due to molecular and Mie scattering. An example of DOAS fit for HONO is presented in Fig. 1.

In the case of NO_2, the 425–490 nm fitting window is used and, in addition to the NO_2 cross-sections at 220 and 296 K (Vandaele et al., 1998), the following trace gas cross-sections are taken into account in the DOAS analysis: O_3 at 241 K (Burrows et al., 1999), O_4 (Hermans et al., 2003), and H_2O (Harder and Brault, 1997). A Ring spectrum and a third-order polynomial closure term are also included. An example of DOAS fit for NO_2 is also shown in Fig. 1.

The O_4 DSCDs needed for the aerosol extinction profile retrieval (see Sect. 2.3) are retrieved in the UV and visible regions (338–370 nm and 425–490 nm, respectively) using the O_4 cross-sections from Hermans et al. (2003). The other DOAS settings are described in Clémer et al. (2010).

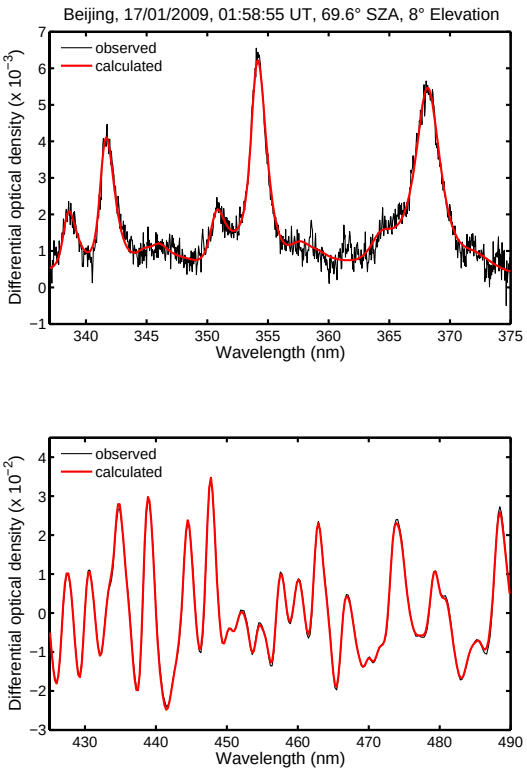

Fig. 1. Example of DOAS fit for HONO (upper plot) and NO_2 (lower plot) at Beijing. Similar DOAS fit results are obtained at Xianghe.

2.3 HONO, NO_2, and aerosol profile retrievals

HONO and NO_2 vertical profiles can be retrieved for each MAX-DOAS scan by applying an inversion algorithm to the corresponding sets of DSCDs measured at the different elevation angles. This profiling technique is based on the fact that the mean scattering height rises into the atmosphere with the increase of the elevation angle and probes the layers where the tropospheric absorber is present. So, each measured DSCD of a MAX-DOAS scan is representative of the absorber concentration in a given altitude range and therefore the observed DSCD variation as a function of the elevation angle depends on the vertical distribution of the absorber. In this study, we used the bePRO inversion algorithm developed at BIRA-IASB (Clémer et al., 2010). It is based on the Optimal Estimation Method (OEM; Rodgers, 2000) and uses a two-step approach. First, the aerosol extinction vertical profiles are retrieved separately at 360 and 477 nm for each MAX-DOAS scan from the corresponding measured O_4 DSCDs. The principle of this retrieval is the following: since the O_4 vertical profile is well-known and nearly constant (it varies with the square of the O_2 monomer concentration), O_4 DSCD measurements can provide information on the vertical distribution of aerosols (Wagner et al., 2004; Friess et al., 2006). This first step is required since the light path length through the atmosphere (and thus the measured HONO or NO_2 DSCD) strongly depends on the aerosols and therefore a good estimate of the vertical distribution of the aerosols is needed to perform accurate HONO and NO_2 profile retrievals. Further details regarding our aerosol retrieval (aerosol optical depth (AOD) and extinction coefficient), including the corresponding bePRO settings, are extensively described in Clémer et al. (2010). The only difference with the latter study is the use of two separate wavelengths (360 nm and 477 nm) instead of four (360, 477, 577, and 630 nm). In the second step, the bePRO algorithm is applied to the measured HONO and NO_2 DSCDs in order to retrieve vertical profiles of these trace gas species. In the OEM, the weighting function matrix ($\mathbf{K}$) and the a priori profile $\boldsymbol{x}_a$ are two important retrieval parameters. $\mathbf{K}$ expresses the sensitivity of the measurements (DSCDs) to changes in the trace gas profile and it is calculated using the linearized discrete ordinate radiative transfer model (LIDORT; Spurr, 2008) as forward model. This code includes an analytical calculation of the weighting functions allowing for near real time automated retrievals without the need of pre-calculated look-up tables. Since the present retrieval problem is ill-conditioned (no unique solution for the trace gas or aerosol extinction vertical profile due to the too small information content of fitted DSCDs from one MAX-DOAS scan), a priori constraints are needed to reject unrealistic solutions and to stabilise the inversion. For HONO and NO_2 vertical profile retrievals, exponentially decreasing a priori profiles have been used with a fixed scaling height of 0.5 km according to the following expression:

$$\boldsymbol{x}_a(z) = \frac{\mathrm{VCD_a}}{\mathrm{SH}} e^{-\frac{z}{\mathrm{SH}}} \quad (1)$$

where $\boldsymbol{x}_a(z)$ is the a priori profile (HONO or NO_2 concentration as a function of the altitude z), SH is the scaling height (fixed to 0.5 km) and $\mathrm{VCD_a}$ is the a priori vertical column density of HONO or NO_2. For each scan, $\mathrm{VCD_a}$ is derived using the geometrical approximation, i.e. the HONO or NO_2 layer is assumed to be located below the scattering altitude at 30° Elevation, so that tropospheric HONO or NO_2 VCDs can be derived by applying a geometrical AMF to measured DSCDs at 30° Elevation (Hönninger et al., 2004; Brinksma et al., 2008).

The other important retrieval parameter settings, which are the a priori and measurement uncertainty covariance matrices ($\mathbf{S}_a$ and $\mathbf{S}_\varepsilon$, respectively), have been constructed as in Clémer et al. (2010). Profile retrievals have been performed at the following wavelengths: 354 nm for HONO and 460 nm for NO_2. The pressure and temperature profiles were taken from the US Standard Atmosphere and the retrieval grid was chosen as in Clémer et al. (2010): ten layers of 200 m thickness between 0 and 2 km, two layers of 500 m between 2 and 3 km and 1 layer between 3 and 4 km.

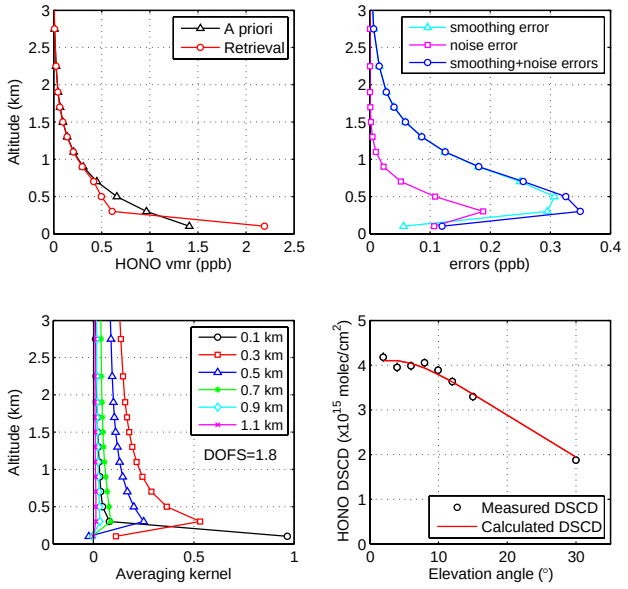

Fig. 2. Example of HONO vertical profile retrieval (Beijing, 21 January 2009, ∼ 10:15 local time). The upper plots display the a priori and retrieved profiles (left) and the smoothing and noise errors (right). Averaging kernels and fit results (comparison between measured DSCDs and those calculated with the retrieved profile) are shown in the lower plots. Error bars on the measured DSCDs are the DOAS fit errors.

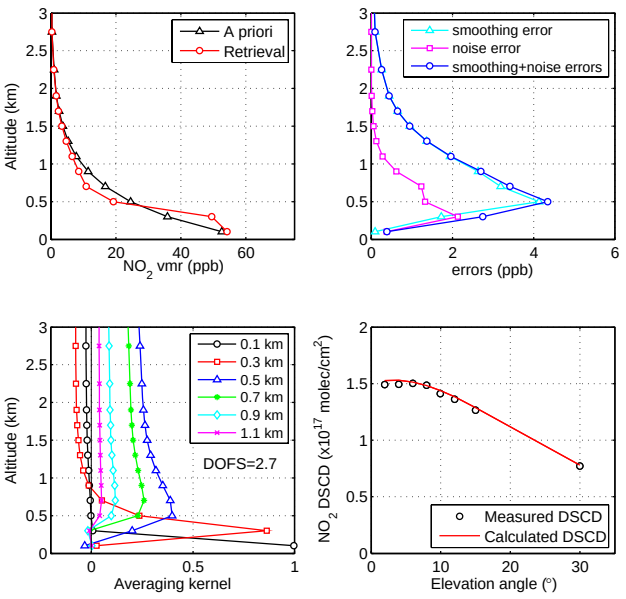

Fig. 3. Same as Fig. 2 but for NO_2.

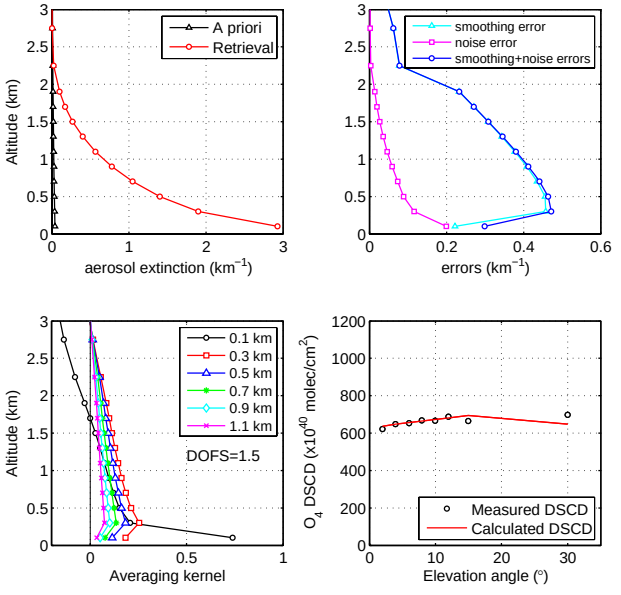

Fig. 4. Same as Figs. 2 and 3 but for aerosol extinction vertical profile retrieved from O_4 DSCDs at 360 nm.

Examples of HONO, NO_2, and aerosol extinction coefficient profile retrievals for winter conditions are presented in Figs. 2, 3, and 4, respectively. The examination of the averaging kernels, which give information on the sensitivity of the retrievals to the vertical distribution, shows that the HONO and aerosols inversions are mostly sensitive close to the surface (0–200 m layer) and to the overhead column above 200 m. In the case of NO_2, three layers can be distinguished: 0–200 m, 200–400 m, and the column above 400 m. It should be noted that a similar vertical sensitivity is obtained for summer conditions. Since our study is mainly focused on HONO, we decided to investigate the HONO and NO_2 concentrations in the 0–200 m layer as well as the vertical column densities of these species. The retrieval of both columns and near-surface concentrations is the main strength of the MAX-DOAS technique: it helps to distinguish between photochemical and vertical transport influences on the diurnal cycle of HONO and NO_2 given that columns are less sensitive than concentrations to the growth of the boundary layer. Regarding the information content, it should be noted that the number of independent pieces of information, also called degrees of freedom for signal (DOFS) and given by the trace of the matrix **A** (Rodgers, 2000), is generally larger for NO_2 than for HONO (2.7 and 1.8 in the examples shown in Figs. 2 and 3). This is due to the fact that the NO_2 absorption strength is larger by more than one order of magnitude than the HONO one, leading to a significantly higher sensitivity of the MAX-DOAS observations to NO_2.

From the error budgets presented in Figs. 2, 3, and 4, the contribution of the smoothing error, which represents the difference between the retrieved profile and the true profile due to vertical smoothing by the retrieval algorithm (Rodgers, 2000), is seen to be significantly larger than the noise (DOAS fit) error, except in the lowest layers. The sum of smoothing and noise errors on the HONO volume mixing ratio (VMR)

Table 1. Error budget of the retrieved HONO and NO_2 near-surface (0–200 m) concentrations and vertical column densities (VCD). The total uncertainty is calculated by adding the different error terms in Gaussian quadrature.

	Beijing				Xianghe			
	0–200 m		VCD		0–200 m		VCD	
	HONO	NO_2	HONO	NO_2	HONO	NO_2	HONO	NO_2
Smoothing + noise errors (%)	19	4	8	3	23	8	10	3
Uncertainty related to the aerosol retrieval (%)	18	21	7	5	21	25	8	6
Uncertainty related to the a priori (%)	7	10	20	10	11	14	23	10
Uncertainty on HONO or NO_2 cross sections (%)	5	3	5	3	5	3	5	3
Total uncertainty (%)	28	24	23	12	33	30	27	12

in the 0–200 m layer and on the HONO vertical columns amount on average to 19 % and 8 %, respectively at Beijing and to 23 % and 10 % at Xianghe. The corresponding values for NO_2 are 4 % and 3 %, respectively at Beijing and 8 % and 3 % at Xianghe. One of the main forward model error sources in HONO and NO_2 profile retrievals is the uncertainty on the retrieved aerosol extinction profiles in step 1. If we combine the smoothing and noise errors on the retrieved aerosol vertical profile (see Fig. 4) to a systematic error of 20 % on O_4 DSCDs (Clémer et al., 2010; Wagner et al., 2009), the corresponding impacts on the HONO and NO_2 retrievals are in the 18–25 % and 5–8 % ranges for surface concentrations and VCDs, respectively. The uncertainty related to the choice of the a priori profile for the HONO and NO_2 retrievals has been estimated by varying the scaling height (SH; see Eq. 1) defining the a priori profile, more precisely, by adopting a value of either 0.5 km (standard retrieval) or 1 km. At Beijing, using a SH value of 1 km instead of 0.5 km leads to the following average changes on the retrieved quantities: -7 and $+10$ % on the HONO and NO_2 near-surface concentrations, respectively, and $+20$ and $+10$ % on the HONO and NO_2 vertical columns, respectively. The corresponding changes for Xianghe are $+11$ and $+14$ % (HONO and NO_2 near-surface concentrations) and $+23$ and $+10$ % (HONO and NO_2 vertical columns). Total uncertainties are estimated by combining the above error sources to the systematic uncertainty on the HONO and NO_2 cross-sections (5 % and 3 %, respectively, according to Stutz et al., 2000 and Vandaele et al., 1998). The error budget on HONO and NO_2 near-surface concentrations and vertical column densities is presented in Table 1.

It is known that clouds and aerosols might bias the MAX-DOAS trace gas retrieval (Wagner et al., 2004; Friess et al., 2006). Instead of explicitly applying a could filtering approach, HONO, NO_2, and aerosol profile retrievals have been quality-checked for each MAX-DOAS scan by comparing the measured DSCDs to those calculated using the retrieved profiles (see examples of retrieval fit results in Figs. 2, 3, and 4 for HONO, NO_2, and aerosols, respectively). In practice, the selection of good profile retrievals is based on the following criteria: (1) residual (RMS) of the retrieval fit smaller than an empirically derived threshold value (3.5×10^{14} molec cm^{-2} for HONO and 2.4×10^{16} molec cm^{-2} for NO_2), (2) DOFS larger than 0.7 meaning that the information comes mainly from the measurements and not from the a priori profile, (3) scans with bad O_4 fit results (RMS of the fit larger than 30 % of the mean O_4 DSCD of the scan), which can be obtained, e.g. for changing aerosol loading or/and cloud conditions during a scan, are rejected, and (4) scans with very large AOD values (> 6) are also rejected given the significantly larger uncertainties on the trace gas retrievals in such conditions. Using these four criteria, about 35 % of the scans are rejected at both stations.

2.4 Verification of the HONO, NO_2 and aerosol retrievals

The NO_2 and aerosol retrievals have been evaluated through comparison with correlative observations. In the case of NO_2, the VCDs retrieved in the Beijing city centre have been compared to MAX-DOAS measurements performed by Ma et al. (2013) at the China Meteorological Administration (39.95° N, 116.32° E) located at about 10 km southwest of the Institute of Atmospheric Physics where our MAX-DOAS spectrometer was installed. It is important to note that both instruments were pointing towards the same direction (North) and that Ma et al. (2013) have used the simple geometrical approximation to derive the NO_2 VCDs (no Optimal Estimation step such as in the present study). Figure 5 shows the comparison of seasonally averaged diurnal variations of the tropospheric NO_2 VCDs for the period August 2008 to April 2009. As can be seen, a very good agreement is obtained, with both MAX-DOAS datasets displaying very similar diurnal variation in both shape and absolute values. In fall and summer, however, our retrieved VCDs are notably noisier than in Ma et al. (2013). It is likely related to the smaller number of available retrievals during these seasons, due to the more strict scan selection criteria imposed in the OEM-based method (see Sect. 2.3) compared to the Ma et al. (2013) approach. Regarding aerosols, AODs at 360 nm retrieved at Beijing and Xianghe have been compared to correlative data from co-located CIMEL sunphotometers of to the AERONET network (http://aeronet.gsfc.nasa.gov). As

Table 2. Compilation of existing daytime (±3 h around local noon) HONO surface concentration measurements performed in or in the vicinity of big cities in East Asia. Beijing and Xianghe values correspond to the present study while other data are taken from Li et al. (2012; see also references therein). PRD is for Pearl River Delta region.

Location	Daytime HONO surface concentration (ppb)
	Spring/summer
Xianghe (China)	0.15
Beijing (China)	0.17
Yufa (China)	0.43
Backgarden (PRD, China)	0.24
Guangzhou (PRD, China)	2.00
Seoul (Korea)	0.36
	Fall/winter
Xianghe (China)	0.40
Beijing (China)	0.55
Shanghai (China)	0.35
Xinken (PRD, China)	0.80
Tokyo (Japan)	0.05

shown in Fig. 6, a good consistency is found between MAX-DOAS and CIMEL instruments at both sites, with correlation coefficients and slopes very close to 1, in agreement with Clémer et al. (2010). These results indicate that the first step of our OEM-based trace gas retrieval, i.e. the aerosol profiling, is robust and reliable.

A thorough validation of HONO retrievals such as those carried out for NO_2 and aerosols is currently not possible due to the lack of correlative datasets at both stations. However, as in Li et al. (2012), MAX-DOAS HONO surface concentrations have been compared to other existing measurements made in or in the vicinity of big cities in East Asia. As can be seen in Table 2, Beijing and Xianghe values are at the low end of existing measurements in spring/summer while they are comprised between the concentrations measured at Shanghai and Xinken (Pearl River Delta region) data in fall/winter. These results show that our MAX-DOAS HONO retrievals at Beijing and Xianghe are reasonably consistent with other existing measurements in East Asia, giving us confidence on the reliability of our HONO datasets. This compilation of HONO measurements also further confirms that the Pearl River Delta region is among the most important HONO hot spots in the world.

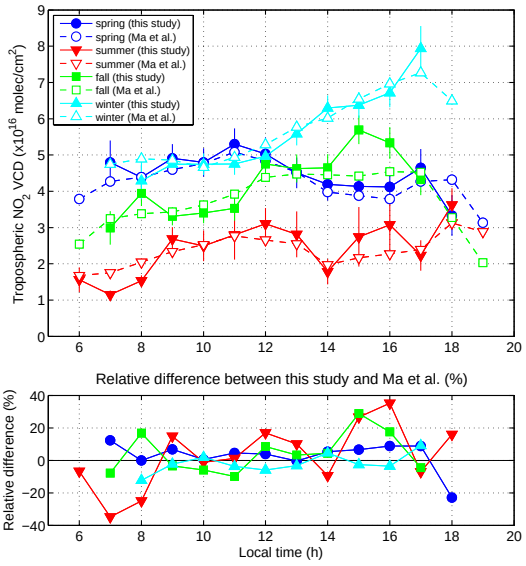

Fig. 5. Comparison of seasonally averaged tropospheric NO_2 VCD diurnal variations from MAX-DOAS measurements performed at the Institute of Atmospheric Physics (present study) and at the China Meteorological Administration (Ma et al., 2013) in the Beijing city centre. The period covered by the observations is August 2008–April 2009. Ma et al. (2013) is taken as reference for the calculation of relative differences. The calculated mean biases are: $+3 \pm 9$ % in spring, $+3 \pm 20$ % in summer, $+4 \pm 12$ % in fall, and -2 ± 6 % in winter.

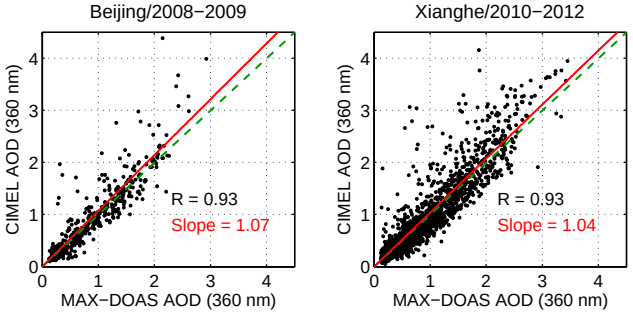

Fig. 6. Scatter plots of the AODs at 360 nm retrieved from MAX-DOAS and sunphotometer measurements at Beijing (left plot, August 2008–April 2009) and Xianghe (right plot, March 2010–December 2012). The linear regressions appear in red and the green dashed lines correspond to the 1 : 1 lines.

3 Results and discussion

3.1 Seasonal variation of daytime HONO, NO_2, and aerosols

Time-series of daytime (local noon) HONO and NO_2 surface concentration and VCD as well as AOD (360 nm) monthly means are presented in Fig. 7. A marked seasonality of the HONO surface concentration and VCD is observed at both stations, with a maximum in late fall/winter and a

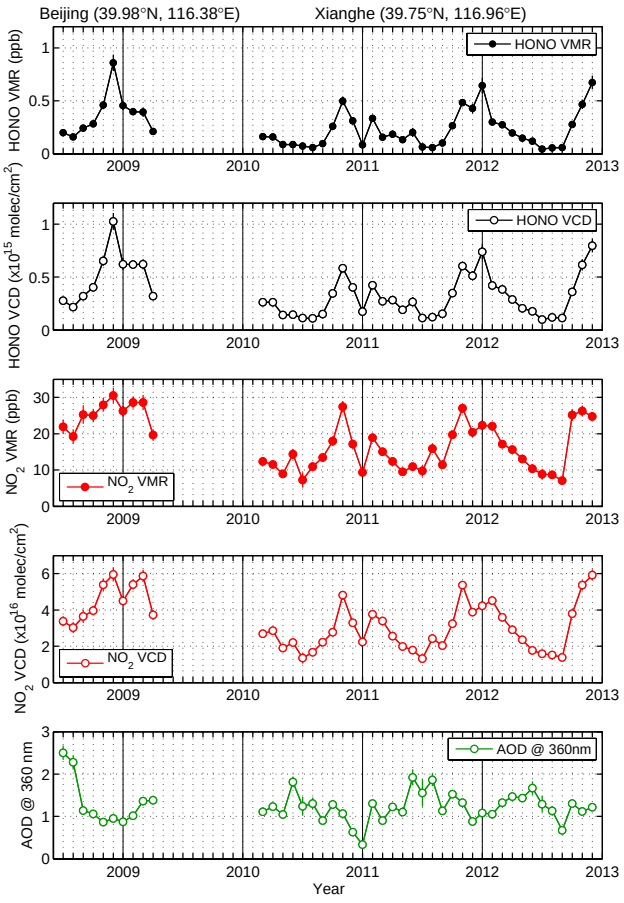

Fig. 7. Time-series of monthly averaged HONO and NO_2 near-surface concentrations (filled circles) and vertical columns (VCD; empty circles) at local noon (±2 h) at Beijing (July 2008–April 2009) and Xianghe (March 2010–December 2012). AODs at 360 nm retrieved from MAX-DOAS measurements appear in the lower plot. The error bars represent the standard deviation of the mean.

minimum in summer. The HONO surface concentration (0–200 m layer) ranges between ∼0.1 and 0.8 ppb in Beijing and between ∼0.03 and 0.7 ppb in Xianghe. These values are consistent with published daytime surface measurements of HONO performed in or in the vicinity of big cities and ranging from 0.05 to 2 ppb (Li et al., 2012), the lowest and highest values having been observed in Tokyo (Kanaya et al., 2007) and in Guangzhou City, South China (Qin et al., 2009), respectively (see also Table 2). From Fig. 7, it is found that the HONO seasonal variation follows well the seasonality of NO_2 which is believed to be its main precursor. The late fall/winter maximum is a well-known feature of NO_2 columns over industrialized areas at mid-latitudes and in particular over Northeastern China (Richter et al., 2005) and is mainly attributed to the longer photochemical lifetimes caused by the winter depletion of OH radical levels (Stavrakou et al., 2013). Domestic heating also contributes to the late fall/winter maximum, but its role is minor due to the dominance of other NO_x sources in Eastern China (Zhang et al., 2007). The HONO seasonality is the result of both enhanced production in winter (due to the NO_2 maximum) and more efficient photolysis in summer. Furthermore, the boundary layer height (BLH) is higher in summer than in winter, about 3 and 1 km in summer and winter, respectively, according to ECMWF ERA-Interim data, leading to a larger dilution of HONO in summer and therefore to lower concentrations close to the surface. This effect seems minor, however, since the seasonal cycle of HONO VCD has an only slightly lower relative amplitude (peak-to-trough ratio between 5 and 10) compared to the near-surface concentration (ratio around 10). Figure 7 also shows that the AOD has a distinct seasonality with a maximum in spring/summer and a minimum in winter. Such a seasonal variation of the AOD over Beijing was also reported by Yu et al. (2009a) using AERONET observations. It can be mainly attributed to particles emitted from massive agricultural fires in the region surrounding Beijing during the May-July period with a peak in June (Xia et al., 2013) as well as to long-range transport of dust particles during spring/summer (Yu et al., 2009a).

Related to Fig. 7, it should be also noted that the corresponding monthly mean DOFS range between 2.0 and 3.0 for NO_2, and 1.8 and 2.2 for aerosols, indicating that the retrieved surface concentration or extinction coefficient is independent from the corresponding VCD or AOD. It is also the case for HONO during the late fall/winter/early spring period with a DOFS around 1.8–2.0. In summer, the DOFS decreases to values around 1.5, suggesting that the surface concentration is to some extent not independent from the retrieved VCD and a priori profile shape. The number of days used for the calculation of monthly means exhibits a similar seasonality with a maximum in fall/winter/early spring (∼25–30 days) and a minimum in summer (∼15 days) due to the low daytime HONO amounts observed during this period making the OEM-based retrieval less stable and leading therefore to a larger number of rejected scans.

The HONO, NO_2, and aerosol seasonal variations at both stations are further illustrated in Fig. 8 where the monthly near-surface concentrations, VCDs, and AODs around local noon have been averaged over the whole measurement period. The HONO concentrations and columns are found to be generally larger at Beijing than at Xianghe, as a result of the larger NO_2 concentrations observed in the Beijing city centre (Figs. 7 and 8). The largest difference between the sites concerns the 90th percentile of HONO surface concentrations (Fig. 8) which can reach up to 2 ppb at Beijing in winter while the corresponding values do not exceed 1.25 ppb for the same period at Xianghe. The heterogeneous conversion of NO_2 into HONO appears to be very probably the dominant source of HONO at both sites and especially in Beijing, given the high correlation coefficient found between HONO and NO_2 near-surface concentrations (R_{HONO/NO_2}) and between HONO concentration and the

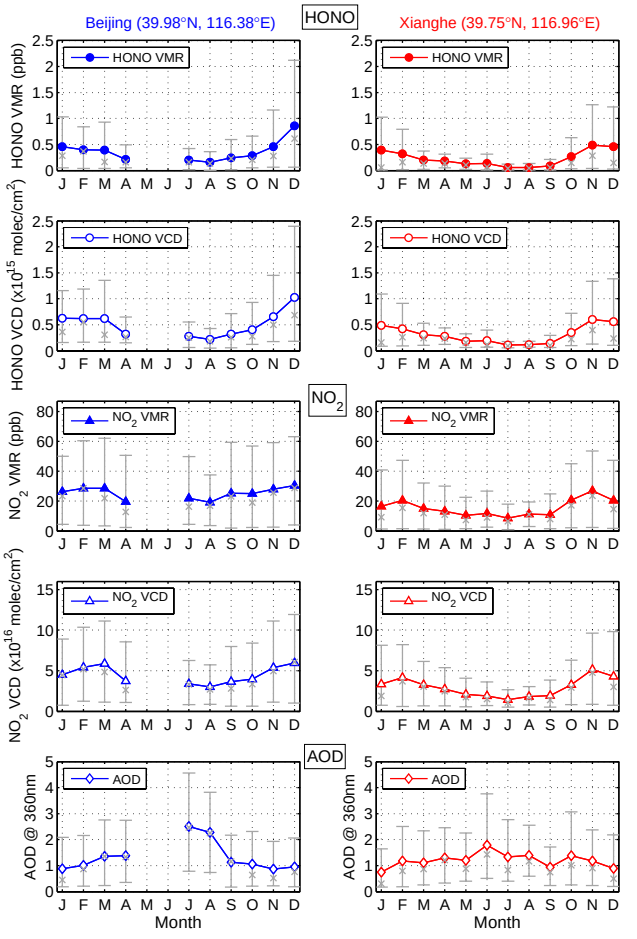

Fig. 8. Seasonal variation of the HONO and NO_2 surface concentration and vertical column density (VCD) and AOD at 360 nm at Beijing (left plots) and Xianghe (right plots). Data correspond to monthly averages over the time interval of ±2 h around local noon. The cross symbol and the lower (upper) error bars represent the median and the 10th (90th) percentiles of the data, respectively.

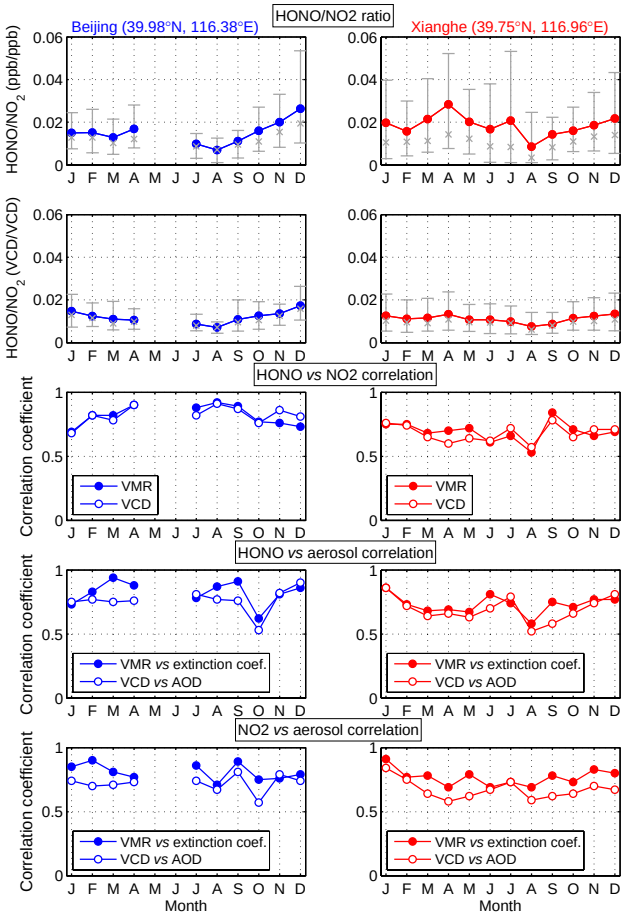

Fig. 9. Seasonal variation of the HONO to NO_2 near-surface concentration ratio, the HONO to NO_2 VCD ratio, and the HONO versus NO_2, HONO versus aerosol, and NO_2 versus aerosol correlation coefficients (0–200 m VMR and vertical column density (VCD)) at local noon at Beijing (left plots) and Xianghe (right plots). In the two upper plots, the cross symbol and the lower (upper) error bars represent the median and the 10th (90th) percentiles of the data, respectively.

aerosol extinction coefficient ($R_{HONO/AERO}$) retrieved in the 0–200 m layer. Figure 9 shows that R_{HONO/NO_2} lies in the range 0.7–0.9 at Beijing and 0.5–0.8 at Xianghe, while the corresponding $R_{HONO/AERO}$ values are comprised between 0.60 and 0.95 and between 0.55 and 0.85, respectively. It should be noted that a strong correlation is also obtained between NO_2 and aerosols in the 0–200 m layer with correlation coefficients ranging between 0.6 and 0.9 at both stations. Similar correlation coefficient values are obtained between integrated concentrations, i.e. between HONO and NO_2 VCDs, between HONO VCD and retrieved AOD, and between NO_2 VCD and retrieved AODs, suggesting that the high correlation obtained for surface concentrations is not due to changes resulting from the variation of the boundary layer height. As can be seen from Fig. 10, the high correlations found between HONO, NO_2, and aerosols are driven at both stations by day-to-day changes: within one month (summer or winter), the short-term variations of the daily means exhibit the same patterns with peaks and troughs on the same days for both trace gases and aerosols. Although a strong correlation is expected between NO_2 and HONO, since NO_2 is recognised as the main precursor of HONO, the same is not true for the correlation between NO_2 and aerosols. Therefore, the high correlation is, more than likely, mainly of meteorological origin, given the relative similarity in the spatial distribution of aerosols and NO_x, which both have a strong anthropogenic component. For HONO and aerosols, the high correlation might be further enhanced by the expected role of aerosols as mediator in the heterogeneous conversion of NO_2 to HONO. Due to the high concentrations of PM_{10} and $PM_{2.5}$ usually observed in the Beijing area, heterogeneous reactions on aerosols have been

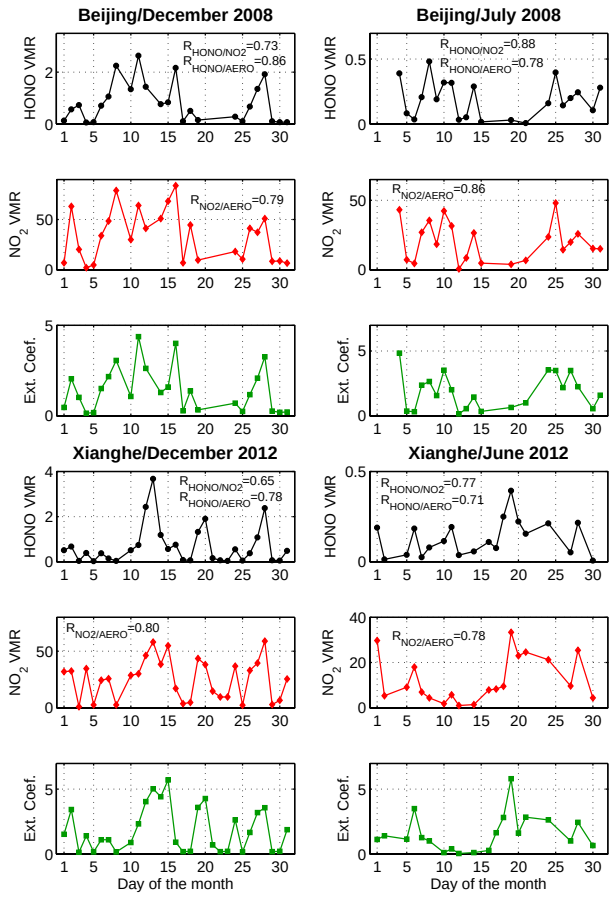

Fig. 10. Day-to-day changes of daytime HONO and NO_2 surface concentrations and aerosol extinction coefficient for one summer and one winter months at both stations. Data correspond to daily averages over the time interval of ± 2 h around local noon. Similar features are obtained for VCDs and AODs. The correlation coefficient values are also given in the figure.

estimated by Li et al. (2011) to contribute as much as $\sim 60\,\%$ to the total HONO production in the Beijing region using a model constrained by observations of HONO, O_3, PM_{10}, and $PM_{2.5}$. A significant role played by PM_{10} is further supported by the high correlation coefficients derived by Qin et al. (2009) from long-path DOAS and particulate monitor measurements in summer in the Guangzhou city, China ($R_{\mathrm{HONO/NO_2}}$ and $R_{\mathrm{HONO/PM_{10}}}$ close or larger than 0.7). In contrast, our $R_{\mathrm{HONO/NO_2}}$ and $R_{\mathrm{HONO/AERO}}$ correlation coefficients are significantly higher than those reported by Li et al. (2012) at a rural site in Southern China in summer ($R_{\mathrm{HONO/NO_2}} \sim 0.4$ and $R_{\mathrm{HONO/AERO}} \sim 0.6$), suggesting that the formation of HONO from NO_2 is more dominant in an urban environment, while other sources (e.g. soil emissions or the photolysis of nitrate and nitric acid deposited on vegetation) appear to play a larger role in rural areas.

The seasonal variation of the ratio of HONO and NO_2 concentrations (HONO / NO_2) at local noon is shown in Fig. 9, and the season-averaged concentrations, vertical columns and ratios are summarised in Tables 3 and 4. The scaling of HONO to NO_2 or NO_x is often used to make the link between HONO and its possible sources, i.e. as an indicator of the efficiency of the conversion of NO_2 into HONO (e.g. Sörgel et al., 2011a; Wojtal et al., 2011; Li et al., 2012). The HONO / NO_2 ratio values are usually sorted into the three following regimes (Wojtal et al., 2011 and references therein): direct emission (HONO / NO_2 less than 0.01) and surface sources in low and high relative humidity environments (HONO / NO_2 in the 0.01–0.03 and 0.03–0.1 ranges, respectively). It should be noted that HONO / NO_2 ratio values up to 0.30 have been derived from nighttime long-path DOAS measurements in Kathmandu, Nepal by Yu et al. (2009b) and were explained by high pollution and relative humidity and low inversion layer. The monthly averaged HONO / NO_2 ratio observed in the 0–200 m layer is comprised on average between 0.007 and 0.028 at both sites (Fig. 9). Although there are significant differences (up to a factor of 2) between the near-surface concentrations ratios observed at Beijing and Xianghe, the VCD ratios are remarkably similar at both sites, and show only little seasonal variations, with values varying between 0.008 in summer and 0.013 in fall and winter (see Table 4 and also Fig. 9). The summertime minimum is consistent with the higher photolytic sink in that season. Higher ratio values are obtained in the 0–200 m layer, by a factor ranging between 1.5 and 2, due to the shorter HONO lifetime and hence the stronger vertical gradients for HONO compared to NO_2 (see e.g. Figs. 2 and 3). Although the photolytic loss of HONO is likely an important driver of these daytime HONO / NO_2 ratios, differences between the seasonal variations of the near-surface concentration ratios at both sites are observed (see Fig. 9), suggesting that other processes can play a significant role. These could be, e.g. differences in vertical mixing or effects of horizontal transport of NO_2, especially during the winter when lifetimes are long. The 90th percentile of the monthly-averaged near-surface HONO / NO_2 ratios indicates that this ratio can reach values of up to about 0.05 at both sites (Fig. 9). The mean and 90th percentile values reported here are consistent with those measured around local noon in big cities and ranging from 0.003 to 0.075 (Li et al., 2012; Elshorbany et al., 2012, and references therein).

3.2 Diurnal variation of HONO and NO_2

Since the MAX-DOAS instrument operates continuously from about 85° SZA sunrise to 85° SZA sunset with a time resolution of ~ 15 min, the diurnal variation of HONO and NO_2 surface concentrations and VCDs can be thoroughly investigated throughout the year at both stations. Figure 11 presents the diurnal variations of HONO and NO_2 surface concentrations and HONO / NO_2 ratios (VMR / VMR) observed at Beijing and Xianghe. Measurements have been averaged per season using 1 h bins.

Table 3. Mean HONO near-surface concentration (VMR in ppb unit) and vertical column density (VCD in 10^{15} molec cm^{-2} units) around local noon (±2 h) at Beijing and Xianghe. The 10th and 90th percentiles of the data are also given.

		Beijing			Xianghe		
		HONO mean	10th perc.	90th perc.	HONO mean	10th perc.	90th perc.
Spring	VMR	0.19	0.04	0.45	0.16	0.03	0.30
	VCD	0.31	0.16	0.58	0.24	0.09	0.41
Summer	VMR	0.18	0.01	0.40	0.09	0.01	0.19
	VCD	0.25	0.05	0.49	0.15	0.06	0.28
Fall	VMR	0.46	0.05	1.14	0.38	0.03	1.01
	VCD	0.60	0.15	1.42	0.48	0.10	1.15
Winter	VMR	0.48	0.04	1.04	0.34	0.02	0.86
	VCD	0.69	0.17	1.33	0.44	0.09	0.96

Table 4. Mean HONO / NO_2 ratio (VMR / VMR and VCD / VCD) around local noon (±2 h) at Beijing and Xianghe. The 10th and 90th percentiles of the data are also given.

		Beijing			Xianghe		
		HONO / NO_2 mean	10th perc.	90th perc.	HONO / NO_2 mean	10th perc.	90th perc.
Spring	VMR	0.015	0.006	0.025	0.024	0.006	0.046
	VCD	0.010	0.006	0.015	0.012	0.006	0.021
Summer	VMR	0.008	0.002	0.013	0.017	0.004	0.035
	VCD	0.008	0.005	0.011	0.009	0.004	0.015
Fall	VMR	0.020	0.007	0.034	0.018	0.006	0.033
	VCD	0.014	0.007	0.023	0.012	0.006	0.021
Winter	VMR	0.015	0.007	0.026	0.020	0.004	0.039
	VCD	0.013	0.007	0.021	0.012	0.005	0.022

The diurnal cycle of NO_2 reflects the balance between anthropogenic emissions and photochemical sinks. In fall/winter, when photochemical activity is weak, accumulation of NO_2 results in a continuous increase of its concentrations during the day, whereas in spring/summer, the diurnal cycle is relatively flat. The diurnal cycle of the HONO concentration in the 0–200 m layer exhibits a maximum in the early morning (1.3–1.6 ppb and 0.7–1.0 ppb at Beijing and Xianghe, respectively) due to the nighttime build-up, followed by a decrease. This decrease continues throughout the day at both stations in fall/winter, while in spring/summer the HONO concentration remains relatively constant from local noon until ∼ 16:00, after which time HONO increases slightly until sunset. This diurnal cycle shape is similar to the cycle observed in several field campaigns (Qin et al., 2009; Li et al., 2012; Elshorbany et al., 2012 and references therein). The morning decrease can be attributed to the increasing HONO photolysis rates and vertical mixing, while the HONO increase in the late afternoon can be caused by the progressive absence of photolytic loss and the decrease of the boundary layer height. However, since the HONO VCD has a very similar diurnal cycle (see Fig. 12), the surface concentration variation during the day is therefore not driven by dilution effects. This is consistent with the study of Qin et al. (2009) which indicated a higher correlation between HONO and NO_2 at Guangzhou than between HONO and CO, the latter being used as a tracer for the transport processes.

As shown in Figs. 11 and 12, the HONO / NO_2 ratio (VMR / VMR and VCD / VCD) has a marked diurnal cycle at both stations with, as for HONO, a maximum in the early morning (ratio values up to ∼ 0.05–0.08 in summer) and a decrease during daytime to values around 0.01–0.02. It should be noted that this diurnal cycle, with the absence of a significant increase of the HONO / NO_2 ratio around local noon, is very similar to the one derived by Qin et al. (2009) from long-path DOAS observations in Guangzhou city.

The corresponding diurnal variations of the AOD are also presented in Fig. 12. There is no marked diurnal cycle, with values around 1–1.5 at both stations, except in Beijing in summer where the AOD increases during the morning, with a maximum value of 3 around 11:00.

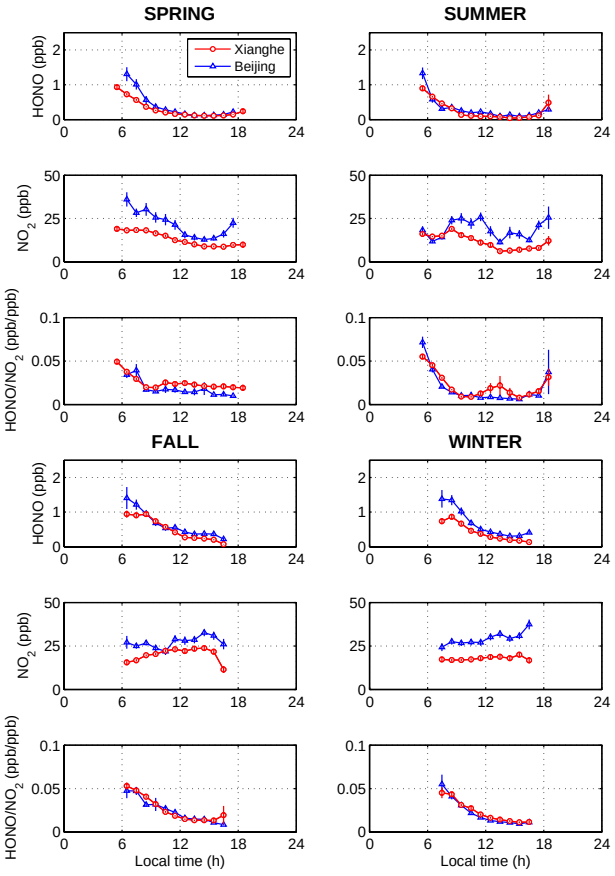

Fig. 11. Diurnal variation of the HONO and NO_2 concentrations (ppb) and their corresponding ratio in the 0–200 m layer at Beijing (blue curves) and Xianghe (red curves). Data have been averaged per season using 1 h bins. The error bars correspond to the standard deviation of the mean.

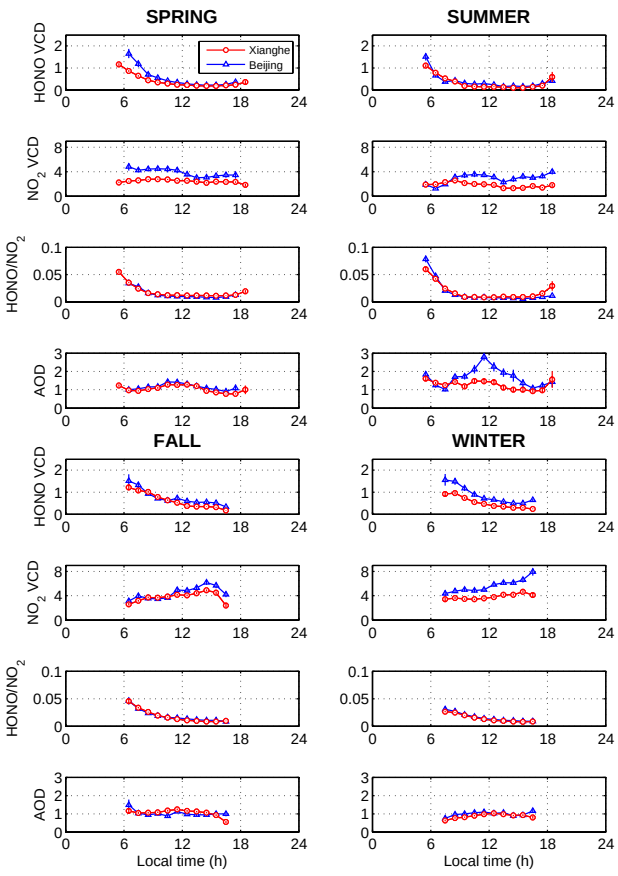

Fig. 12. Same as Fig. 11 but for the vertical column densities (VCDs) and aerosol optical depths (AODs). HONO and NO_2 VCDs are in $\times 10^{15}$ and $\times 10^{16}$ molec cm^{-2} units, respectively. The corresponding diurnal variations of the AOD are also plotted.

3.3 Estimation of OH production from HONO

In order to evaluate the importance of HONO as a source of OH radicals, especially compared to the contribution of O_3 photolysis, the OH production from HONO has been calculated in the 0–200 m layer at both stations from the retrieved HONO concentrations and simulated photolysis rates J (HONO). OH is formed from O_3 through the following reaction sequence:

$$O_3 + h\nu(\lambda < 340\,\text{nm}) \rightarrow O(^1D) + O_2 \quad \text{(R5)}$$

$$O(^1D) + H_2O \rightarrow 2OH \quad \text{(R6)}$$

The corresponding OH production has been estimated from an assumed O_3 concentration fixed to 30 ppb, water vapour concentration from ECMWF (European Centre for Medium-Range Weather Forecasts) ERA-Interim re-analysis fields (http://www.ecmwf.int/research/era/do/get/index), and simulated photolysis rate J ($O_3 \rightarrow O(^1D)$). Since the value of 30 ppb for O_3 is significantly smaller than the afternoon O_3 concentrations (up to 60 ppb) observed in summer (Lu et al., 2013; Wu et al., 2011), we tested the impact of using the diurnal cycle of O_3 measured by Chou et al. (2011) in the Beijing city centre during CAREBeijing-2006. Photolysis rates have been calculated using the TUV package including the SDISORT radiative transfer code (Madronich and Hocke, 1998). The effects of clouds are ignored, whereas attenuation by aerosols is estimated from the aerosol optical depths retrieved by MAX-DOAS at Beijing and Xianghe (see Sect. 2.3), assuming a single scattering albedo equal to 0.9 and an asymmetry parameter equal to 0.7. The albedo is set to 0.05, except over snow (0.5). Snow presence and ozone total columns are obtained from ECMWF ERA-Interim fields.

The calculated photolysis rates are presented in Fig. 13. The J (HONO) values are consistent with those measured by Li et al. (2012) in the Pearl River Delta region in Southern China, and correspond to a noon photolytic lifetime of about 15–20 min, with little differences between the seasons. The diurnal cycles of OH production due to HONO and O_3 are depicted in Fig. 14. At both stations, the OH production from HONO in the 0–200 m layer exhibits a maximum

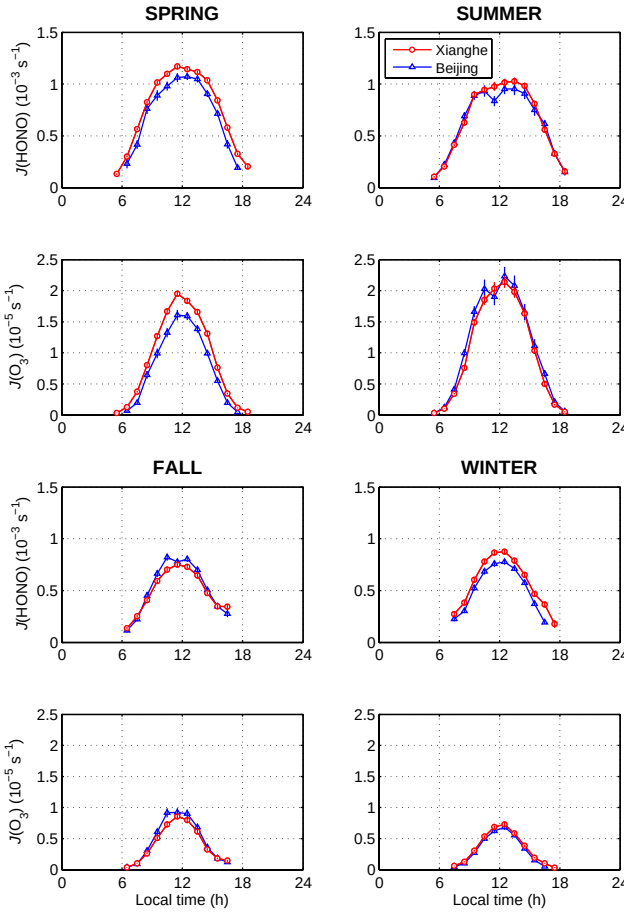

Fig. 13. Photolysis rates J (HONO) and J ($O_3 \rightarrow O(^1D)$) calculated in the 0–200 m layer for Beijing and Xianghe and averaged per season. The error bars correspond to the standard deviation of the mean.

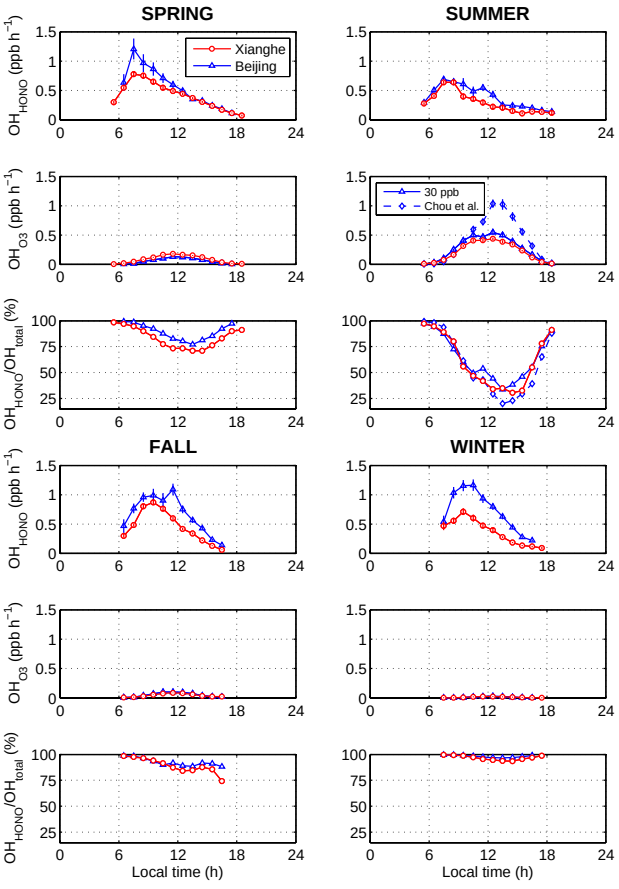

Fig. 14. Diurnal variation of the OH production from HONO (OH_{HONO}) and O_3 (OH_{O_3}) in the 0–200 m layer at Beijing (blue curves) and Xianghe (red curves). Data have been seasonally averaged using 1 h bins. The relative contribution of HONO to the OH production (OH_{HONO}/OH_{total}) is calculated as $OH_{HONO}/(OH_{HONO}+OH_{O_3})$. The error bars correspond to the standard deviation of the mean.

in the morning, between 07:00 and 09:00 in spring/summer and between 08:00 and 11:00 in fall/winter. This maximum is larger at Beijing than at Xianghe, with e.g. winter values reaching 1.2 ppb h^{-1} and 0.7 ppb h^{-1}, respectively, due to the generally larger HONO concentration observed in Beijing (Fig. 11). The shape of this diurnal cycle is similar to the one calculated by Sörgel et al. (2011b) from HONO measurements over a pine forest close to the industrial area of Huelva, southwestern Spain in fall. However, the maximum of OH production from HONO was significantly lower there ($\sim$ 0.2 ppb h^{-1}).

Comparison of the HONO and O_3 contributions to OH production reveals that HONO is the main contributor in all seasons except summer, with relative HONO contributions larger than 70 % (more than 90 % in winter) around 12:00–13:00. In summer, the contribution of O_3 dominates between 09:30 and 16:00 with a maximum of 70 % around 13:00–14:00. At Beijing, this feature is strengthened by considering the diurnal cycle of the ozone concentration measured by Chou et al. (2011) with high afternoon ozone mixing ratios, and very low values in the early morning. In that case, the contribution of O_3 to OH production reaches a maximum of 80 % in the early afternoon.

The seasonal variation of the HONO and O_3 contributions at local noon is displayed in Fig. 15. It is largely explained by the seasonal cycle of ozone photolysis rates (Fig. 13) and H_2O concentrations, which both maximise in summer. These results show that near to the ground surface in urban areas, HONO is the main source of OH radicals in winter as well as in the early morning at all seasons, in agreement with our current knowledge of the HONO photochemistry (see e.g. Li et al., 2012 and references therein).

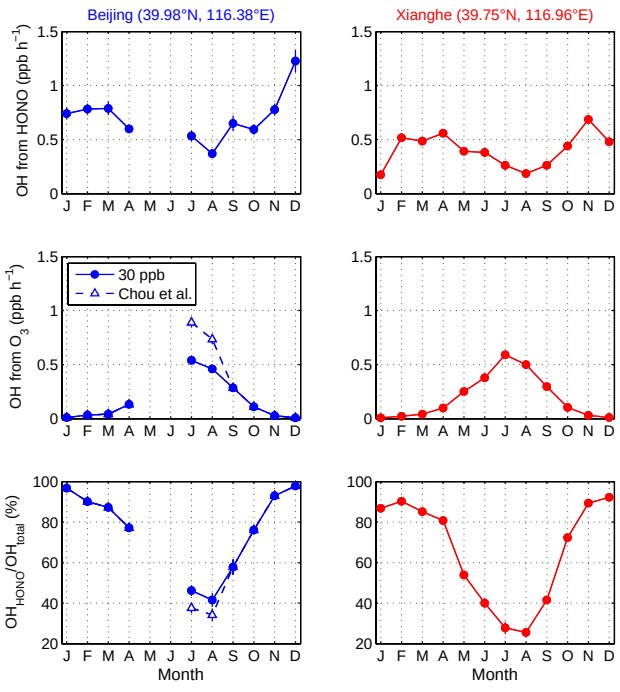

Fig. 15. Seasonal variation of the OH production from HONO (OH_{HONO}) and O_3 (OH_{O_3}) in the 0–200 m layer at Beijing (left/blue curves) and Xianghe (right/red curves) at local noon. Data correspond to monthly averages over the time interval of ±2 h around local noon. OH_{total} is equal to $OH_{HONO} + OH_{O_3}$. The error bars correspond to the standard deviation of the mean.

4 Summary and conclusions

For the first time, the seasonal variation of HONO has been investigated in and in the vicinity of a megacity. This has been achieved using MAX-DOAS observations of HONO and its main precursor NO_2 and aerosols in the Beijing city centre and at the suburban site of Xianghe located ∼ 60 km east of Beijing. The MAX-DOAS spectrometers have the advantage that they can be operated year-round during daytime in a fully automated way. Moreover, independent information on the near-surface concentration and vertical columns of trace gases can be retrieved from multiple elevation angle observations using dedicated inversion methods like the OEM used here. Our instrument was operated in the Beijing city centre from July 2008 until April 2009, and in Xianghe from March 2010 until now. The total error on retrieved near-surface concentrations and vertical columns are comprised between 23 and 33 % for HONO and between 12 and 30 % for NO_2. Retrieved NO_2 VCDs and AODs are also shown to be in good agreement with correlative measurements. In the case of HONO surface concentration, a reasonably good consistency is found between our retrievals and measurements performed in or in the vicinity of big cities in East Asia.

HONO and NO_2 concentrations retrieved at both stations around local noon in the 0–200 m layer exhibit the same marked seasonality, with a maximum in late fall/winter and a minimum in summer. The strong link between HONO and NO_2 is further supported by the high correlation of HONO with NO_2 found throughout the year, with coefficients comprised in the 0.7–0.9 and 0.5–0.8 ranges at Beijing and Xianghe, respectively. Like NO_2, HONO is more abundant at Beijing than at Xianghe, with mean VMR ranging from ∼ 0.1 to 0.8 ppb and from ∼ 0.03 to 0.7 ppb, respectively. These values are found to be consistent with previously reported daytime HONO measurements in urban conditions. A strong role of NO_2 conversion to HONO at Beijing is suggested from the higher correlation coefficients between HONO and aerosol extinctions retrieved in the 0–200 m layer at Beijing (ranging from 0.60 to 0.95 instead of 0.55 to 0.85 at Xianghe).

The diurnal profiles of HONO surface concentration and vertical column show a maximum in the early morning (1.3–1.6 ppb/1.5–1.8 × 10^{15} molec cm^{-2} in Beijing and 0.7–1.0 ppb/0.9–1.1 × 10^{15} molec cm^{-2} in Xianghe) likely explained by the photolysis of the HONO accumulated during the night. The subsequent decrease (to about 0.1–0.4 ppb for the concentration and 0.1–0.6 × 10^{15} molec cm^{-2} for the vertical column around local noon) results mostly from a balance between HONO sources and the photolytic sink. Dilution effects appear to play only a minor role, given the observed very similar diurnal cycle of the HONO vertical column, which is expected to be insensitive to vertical transport variations. The observed HONO / NO_2 ratio diurnal cycle is very similar at both Beijing and Xianghe with a maximum in the early morning (values up to 0.08) and subsequent decreases to values ranging between 0.01 and 0.02 around local noon.

The production of OH radicals from HONO and O_3 has been estimated from observed HONO near-surface concentrations and calculated photolysis rates. At both stations, HONO is found to be the main contributor to OH production in the 0–200 m layer, except in summer around local noon where the contribution of O_3 dominates. The diurnal cycle of the OH production from HONO exhibits a maximum in the morning between 07:00 and 11:00, depending on season, followed by a rapid decrease. This maximum is larger at Beijing than at Xianghe, especially in winter time where the OH production from HONO reaches ∼ 1.2 ppb h^{-1} and ∼ 0.7 ppb h^{-1}, respectively.

To conclude, MAX-DOAS is shown to be a useful technique for long-term monitoring HONO near-surface concentrations and vertical column amounts in polluted areas. Multi-year data sets of HONO observations, such presented in this work, offer a better quantitative characterisation of HONO photochemistry and can provide additional constraints to modelling studies. For example, the diurnal and seasonal profiles of the HONO / NO_2 ratio derived in this study could be used in atmospheric models to constrain the rate of heterogeneous conversion of NO_2 to HONO, in order

to investigate the possible effects of this HONO source on the budget of oxidants.

Acknowledgements. This research was financially supported at IASB-BIRA by the Belgian Federal Science Policy Office, Brussels (PRODEX contract A3C and AGACC-II project), the EU 7th Framework Programme projects NORS (contract 284421) and SHIVA (contract 226224), and the ESA CEOS Intercalibration project (ESA/ESRIN Contract 22202/09/I-EC). We also acknowledge M. Bauwens (BIRA-IASB) for her technical support as well as R. McLaren (York University; Editor of this paper) and two anonymous referees for their helpful comments.

Edited by: R. McLaren

References

Brion, J., Chakir, A., Charbonnier, J., Daumont, D., Parisse, C., and Malicet, J.: Absorption Spectra Measurements for the Ozone Molecule in the 350–830 nm Region, J. Atmos. Chem., 30, 291–299, doi:10.1023/A:1006036924364, 2004.

Brinksma, E. J., Pinardi, G., Volten, H., Braak, R., Richter, A., Schönhardt, A., Van Roozendael, M., Fayt, C., Hermans, C., Dirksen, R. J., Vlemmix, T., Berkhout, A. J. C., Swart, D. P. J., Oetjen, H., Wittrock, F., Wagner, T., Ibrahim, O. W., de Leeuw, G., Moerman, M., Curier, R. L., Celarier, E. A., Cede, A., Knap, W. H., Veefkind, J. P., Eskes, H. J., Allaart, M., Rothe, R., Piters, A. J. M., and Levelt, P. F.: The 2005 and 2006 DANDELIONS NO_2 and aerosol intercomparison campaigns, J. Geophys. Res., 113, D16S46, doi:10.1029/2007JD008808, 2008.

Burrows, J. P., Richter, A., Dehn, A., Deters, B., Himmelmann, S., Voigt, S., and Orphal, J.: Atmospheric Remote-sensing reference data from GOME - 2.Temperature-dependent absorption cross-sections of O_3 in the 231–794 nm range, J. Quant. Spectrosc. Radiat. Transfer, 61, 509–517, 1999.

Chou, C. C.-K., Tsai, C.-Y., Chang, C.-C., Lin, P.-H., Liu, S. C., and Zhu, T.: Photochemical production of ozone in Beijing during the 2008 Olympic Games, Atmos. Chem. Phys., 11, 9825–9837, doi:10.5194/acp-11-9825-2011, 2011.

Clémer, K., Van Roozendael, M., Fayt, C., Hendrick, F., Hermans, C., Pinardi, G., Spurr, R., Wang, P., and De Mazière, M.: Multiple wavelength retrieval of tropospheric aerosol optical properties from MAXDOAS measurements in Beijing, Atmos. Meas. Tech., 3, 863–878, doi:10.5194/amt-3-863-2010, 2010.

Elshorbany, Y. F., Steil, B., Brühl, C., and Lelieveld, J.: Impact of HONO on global atmospheric chemistry calculated with an empirical parameterization in the EMAC model, Atmos. Chem. Phys., 12, 9977–10000, doi:10.5194/acp-12-9977-2012, 2012.

Fleischmann, O. C., Hartmann, M., Burrows J. P., and Orphal, J.: New ultraviolet absorption cross-sections of BrO at atmospheric temperatures measured by time-windowing Fourier transform spectroscopy, J. Photochem. Photobiol. A, 168, 117–132 , 2004.

Friess, U., Monks, P. S., Remedios, J. J., Rozanov, A., Sinreich, R., Wagner, T., and Platt, U.: MAX-DOAS O_4 measurements: A new technique to derive information on atmospheric aerosols: 2. Modeling studies, J. Geophys. Res. 111, D14203, doi:10.1029/2005JD006618, 2006.

George, C., Strekowski, R. S., Kleffmann, J., Stemmler, K., and Ammann, M.: Photoenhanced uptake of gaseous NO_2 on solid organic compounds: a photochemical source of HONO?, Faraday Discuss., 130, 195–210, doi:10.1039/B417888M, 2005.

Grainger, J. and Ring, J.: Anomalous Fraunhofer line profiles, Nature, 193, 762, 1962.

Harder, J. W. and Brault, J. W.: Atmospheric measurements of water vapor in the 442-nm region, J. Geophys. Res., 102, 6245–6252, 1997.

Heland, J., Kleffmann, J., Kurtenbach, R., and Wiesen, P.: A new instrument to measure gaseous nitrous acid (HONO) in the atmosphere, Environ. Sci. Technol., 35, 3207–3212, 2001.

Hendrick, F., Barret, B., Van Roozendael, M., Boesch, H., Butz, A., De Mazière, M., Goutail, F., Hermans, C., Lambert, J.-C., Pfeilsticker, K., and Pommereau, J.-P.: Retrieval of nitrogen dioxide stratospheric profiles from ground-based zenith-sky UV-visible observations: validation of the technique through correlative comparisons, Atmos. Chem. Phys., 4, 2091–2106, doi:10.5194/acp-4-2091-2004, 2004.

Hermans, C., Vandaele, A. C., Fally, S., Carleer, M., Colin, R., Coquart, B., Jenouvrier, A., and Mérienne, M.-F.: Absorption cross-section of the collision-induced bands of oxygen from the UV to the NIR, in: Proceedings of the NATO Advanced Research Workshop, Weakly Interacting Molecular Pairs: Unconventional Absorbers of Radiation in the Atmosphere, Fontevraud, France, 24 April–2 May 2002, edited by: Camy-Peyret, C. and Vigasin, A. A., NATO Science Series IV Earth and Environmental Sciences, vol. 27, Kluwer Academic Publishers, Boston, 193–202, 2003.

Hönninger, G., von Friedeburg, C., and Platt, U.: Multi axis differential optical absorption spectroscopy (MAX-DOAS), Atmos. Chem. Phys., 4, 231–254, doi:10.5194/acp-4-231-2004, 2004.

Kanaya, Y., Cao, R., Akimoto, H., Fukuda, M., Komazaki, Y., Yokouchi, Y., Koike, M., Tanimoto, H., Takegawa, N., and Kondo, Y.: Urban photochemistry in central Tokyo: 1. Observed and modeled OH and HO_2 radical concentrations during the winter and summer of 2004, J. Geophys. Res., 112, D21312, doi:10.1029/2007jd008670, 2007.

Kleffmann, J., Heland, J., Kurtenbach, R., Lörzer, J., and Wiesen, P.: A new instrument (LOPAP) for the detection of nitrous acid (HONO), Environ. Sci. Pollut. R., 4, 48–54, 2002.

Kleffmann, J., Gavriloaiei, T., Hofzumahaus, A., Holland, F., Koppmann, R., Rupp, L., Schlosser, E., Siese, M., and Wahner, A.: Daytime formation of nitrous acid: A major source of OH radicals in a forest, Geophys. Res. Lett., 32, L05818, doi:10.1029/2005GL022524, 2005.

Li, Y., An, J., Min, M., Zhang, W., Wang, F., and Xie, P.: Impacts of HONO sources on the air quality in Beijing, Tianjin, and Hebei Province of China, Atmos. Environ., 45, 4735–4744, 2011.

Li, X., Brauers, T., Häseler, R., Bohn, B., Fuchs, H., Hofzumahaus, A., Holland, F., Lou, S., Lu, K. D., Rohrer, F., Hu, M., Zeng, L. M., Zhang, Y. H., Garland, R. M., Su, H., Nowak, A., Wiedensohler, A., Takegawa, N., Shao, M., and Wahner, A.: Exploring the atmospheric chemistry of nitrous acid (HONO) at a rural site in Southern China, Atmos. Chem. Phys., 12, 1497–1513, doi:10.5194/acp-12-1497-2012, 2012.

Lu, K. D., Hofzumahaus, A., Holland, F., Bohn, B., Brauers, T., Fuchs, H., Hu, M., Häseler, R., Kita, K., Kondo, Y., Li, X., Lou, S. R., Oebel, A., Shao, M., Zeng, L. M., Wahner, A., Zhu, T.,

Zhang, Y. H., and Rohrer, F.: Missing OH source in a suburban environment near Beijing: observed and modelled OH and HO_2 concentrations in summer 2006, Atmos. Chem. Phys., 13, 1057–1080, doi:10.5194/acp-13-1057-2013, 2013.

Ma, J. Z., Beirle, S., Jin, J. L., Shaiganfar, R., Yan, P., and Wagner, T.: Tropospheric NO_2 vertical column densities over Beijing: results of the first three years of ground-based MAX-DOAS measurements (2008–2011) and satellite validation, Atmos. Chem. Phys., 13, 1547–1567, doi:10.5194/acp-13-1547-2013, 2013.

Madronich, S. and Flocke, S.: The role of solar radiation in atmospheric chemistry, in: Handbook of Environmental Chemistry, edited by: Boule, P., Springer-Verlag, Heidelberg, 1–26, 1998.

Meller, R. and Moortgat, G. K.: Temperature dependence of the absorption cross sections of formaldehyde between 223 and 323K in the wavelength range 225–375 nm, J. Geophys. Res., 105, 7089–7101, 2000.

Perner, D. and Platt, U.: Detection of nitrous acid in the atmosphere by differential optical absorption, Geophys. Res. Lett., 6, 917–920, 1979.

Peters, E., Wittrock, F., Großmann, K., Frieß, U., Richter, A., and Burrows, J. P.: Formaldehyde and nitrogen dioxide over the remote western Pacific Ocean: SCIAMACHY and GOME-2 validation using ship-based MAX-DOAS observations, Atmos. Chem. Phys., 12, 11179–11197, doi:10.5194/acp-12-11179-2012, 2012.

Platt, U. and Stuz, J.: Differential Optical Absorption Spectroscopy (DOAS), Principles and Applications, ISBN 978-3-540-21193-8, Springer, Berlin-Heidelberg, 2008.

Qin, M., Xie, P., Su, H., Gu, J., Peng, F., Li, S., Zeng, L., Liu, J., Liu, W., and Zhang, Y.: An observational study of the HONO-NO_2 coupling at an urban site in Guangzhou City, South China, Atmos. Environ., 43, 5731–5742, doi:10.1016/j.atmosenv.2009.08.017, 2009.

Richter, A., Burrows, J. P., Nüss, H., Granier, C., and Niemeier, U.: Increase in tropospheric nitrogen dioxide over China observed from space, Nature, 437, 129–132, doi:10.1038/nature04092, 2005.

Rodgers, C. D.: Inverse Methods for Atmospheric Sounding, Theory and Practice. World Scientific Publishing, Singapore-NewJersey-London-Hong Kong, 2000.

Sörgel, M., Trebs, I., Serafimovich, A., Moravek, A., Held, A., and Zetzsch, C.: Simultaneous HONO measurements in and above a forest canopy: influence of turbulent exchange on mixing ratio differences, Atmos. Chem. Phys., 11, 841–855, doi:10.5194/acp-11-841-2011, 2011a.

Sörgel, M., Regelin, E., Bozem, H., Diesch, J.-M., Drewnick, F., Fischer, H., Harder, H., Held, A., Hosaynali-Beygi, Z., Martinez, M., and Zetzsch, C.: Quantification of the unknown HONO daytime source and its relation to NO_2, Atmos. Chem. Phys., 11, 10433–10447, doi:10.5194/acp-11-10433-2011, 2011b.

Spurr, R., LIDORT and VLIDORT: Linearized pseudo-spherical scalar and vector discrete ordinate radiative transfer models for use in remote sensing retrieval problems, Light Scattering Reviews, Volume 3, edited by: Kokhanovsky, A., Springer, 2008.

Stavrakou, T., Müller, J.-F., Boersma, K. F., van der A, R. J., Kurokawa, J., Ohara, T., and Zhang, Q.: Key chemical NO_x sink uncertainties and how they influence top-down emissions of nitrogen oxides, Atmos. Chem. Phys., 13, 9057–9082, doi:10.5194/acp-13-9057-2013, 2013.

Stemmler, K., Ammann, M., Donders, C., Kleffmann, J., and George, C.: Photosensitized reduction of nitrogen dioxide on humic acid as a source of nitrous acid, Nature, 440, 195–198, doi:10.1038/nature04603, 2006.

Stutz, J., Kim, E. S., Platt, U., Bruno, P., Perrino, C., and Febo, A.: UV-vis Absorption Cross-Section of Nitrous Acid, J. Geophys. Res., 105, 14585–14592, 2000.

Stutz, J., Alicke, B., and Neftel, A.: Nitrous acid formation in the urban atmosphere: Gradient measurements of NO_2 and HONO over grass in Milan, Italy, J. Geophys. Res., 107, 8192, doi:10.1029/2001JD000390, 2002.

Su, H., Cheng, Y., Oswald, R., Behrendt, T., Trebs, I., Meixner, F. X., Andreae, M. O., Cheng, P., Zhang, Y., and Pöschl, U., Soil nitrite as a source of atmospheric HONO and OH radicals, Science, 333, 1616, doi:10.1126/science.1207687, 2011.

Vandaele, A. C., Hermans, C., Simon, P. C., Carleer, M., Colin, R., Fally, S., Mérienne, M.-F., Jenouvrier, A., and Coquart, B.: Measurements of the NO_2 absorption cross section from 42000 cm^{-1} to 10000 cm^{-1} (238–1000 nm) at 220 K and 294 K, J. Quant. Spectrosc. Radiat. Transfer, 59, 171–184, 1998.

Villena, G., Kleffmann, J., Kurtenbach, R., Wiesen, P., Lissi, E., Rubio, M., Croxatto, G., and Rappenglück, B.: Vertical gradients of HONO, NO_x and O_3 in Santiago de Chile, Atmos. Environ., 45, 3867–3873, doi:10.1016/j.atmosenv.2011.01.073, 2011.

Vlemmix, T., Piters, A. J. M., Berkhout, A. J. C., Gast, L. F. L., Wang, P., and Levelt, P. F.: Ability of the MAX-DOAS method to derive profile information for NO_2: can the boundary layer and free troposphere be separated?, Atmos. Meas. Tech., 4, 2659–2684, doi:10.5194/amt-4-2659-2011, 2011.

Wagner T., Dix, B., von Friedeburg, C., Friess, U., Sanghavi, S., Sinreich, R., and Platt, U.: MAX-DOAS O_4 measurements: A new technique to derive information on atmospheric aerosols – Principles and information content, J. Geophys. Res. 109, D22205, doi:10.1029/2004JD004904, 2004.

Wagner, T., Deutschmann, T., and Platt, U.: Determination of aerosol properties from MAX-DOAS observations of the Ring effect, Atmos. Meas. Tech., 2, 495–512, doi:10.5194/amt-2-495-2009, 2009.

Wittrock, F., Oetjen, H., Richter, A., Fietkau, S., Medeke, T., Rozanov, A., and Burrows, J. P.: MAX-DOAS measurements of atmospheric trace gases in Ny-Ålesund – Radiative transfer studies and their application, Atmos. Chem. Phys., 4, 955–966, doi:10.5194/acp-4-955-2004, 2004.

Wang, S., Ackermann, R., and Stutz, J.: Vertical profiles of O_3 and NO_x chemistry in the polluted nocturnal boundary layer in Phoenix, AZ: I. Field observations by long-path DOAS, Atmos. Chem. Phys., 6, 2671–2693, doi:10.5194/acp-6-2671-2006, 2006.

Wong, K. W., Tsai, C., Lefer, B., Haman, C., Grossberg, N., Brune, W. H., Ren, X., Luke, W., and Stutz, J.: Daytime HONO vertical gradients during SHARP 2009 in Houston, TX, Atmos. Chem. Phys., 12, 635–652, doi:10.5194/acp-12-635-2012, 2012.

Wojtal, P., Halla, J. D., and McLaren, R.: Pseudo steady states of HONO measured in the nocturnal marine boundary layer: a conceptual model for HONO formation on aqueous surfaces, Atmos. Chem. Phys., 11, 3243–3261, doi:10.5194/acp-11-3243-2011, 2011.

Wu, Q. Z., Wang, Z. F., Gbaguidi, A., Gao, C., Li, L. N., and Wang, W.: A numerical study of contributions to air pollution in Bei-

jing during CAREBeijing-2006, Atmos. Chem. Phys., 11, 5997–6011, doi:10.5194/acp-11-5997-2011, 2011.

Xia, X., Zong, X., and Sun, Li: Exceptionally active agricultural fire season in mid-eastern China in June 2012 and its impact on atmospheric environment, J. Geophys. Res. Atmos., 118, 9889–9900, doi:10.1002/jgrd.50770, 2013.

Young, C. J., Washenfelder, R. A., Roberts, J. M., Mielke, L. H., Osthoff, H. D., Tsai, C., Pikelnaya, O., Stutz, J., Veres, P. R., Cochran, A. K., VandenBoer, T. C., Flynn, J., Grossberg, N., Haman, C. L., Lefer, B., Stark, H., Graus, M., de Grouw, J., Gilman, J. B., Kuster, W. C., and Brown, S. S.: Vertically resolved measurements of nighttime radical reservoirs in Los Angeles and their contribution to the urban radical budget, Environ. Sci. Technol., 46, 10965–10973, doi:10.1021/es302206a, 2012.

Yu, X., Zhu, B., and Zhang, M.: Seasonal variability of aerosol optical properties over Beijing, Atmos. Environ., 43, 4095–4101, 2009a.

Yu, Y., Galle, B., Panday, A., Hodson, E., Prinn, R., and Wang, S.: Observations of high rates of NO_2-HONO conversion in the nocturnal atmospheric boundary layer in Kathmandu, Nepal, Atmos. Chem. Phys., 9, 6401–6415, doi:10.5194/acp-9-6401-2009, 2009b.

Zhang, Q., Streets, D. G., He, K., Wang, Y., Richter, A., Burrows, J. P., Uno, I., Jang, C. J., Chen, D., Yao, Z., and Lei, Y.: NO_x emission trends for China, 1995-2004: The view from the ground and the view from space, J. Geophys. Res., 112, D22306, doi:10.1029/2007JD008684, 2007.

Zhou, X., Gao, H., He, Y., Huang, G., Bertman, S. B., Civerolo, K., and Schwab, J.: Nitric acid photolysis on surfaces in low-NO_x environments: significant atmospheric implications, Geophys. Res. Lett., 30, 2217, doi:10.1029/2003gl018620, 2003.